This is a repository copy of *Multimode morphodynamic model for sediment-laden flows and geomorphic impacts*.

# A multi-mode morphodynamic model for sediment-laden flows and geomorphic impacts

Mingfu Guan [1*]; Nigel G. Wright, F.ASCE[2]; and P. Andrew Sleigh [3]

**Abstract:** Sediment-laden flows are a complex solid-fluid interaction process. This study presents a multi-mode morphodynamic model system combined with shallow water theory and a non-equilibrium assumption for sediment transport. The model system aims to simulate the morphological change caused by sediment-laden flows with various sediment transport modes. The model involves three modules named: hydrodynamic module, sediment transport module, and morphological evolution module. The hydrodynamic model is governed by modified shallow water equations considering the interaction effects of flow and sediment. A flexible sediment transport model is presented by incorporating a weight coefficient. The model can adaptively choose an appropriate transport mode according to the local, real-time flow conditions. Bedload, suspended load and total mixed sediment load are all involved. The model is solved by a second-order Godunov-type finite volume method which is robust and accurate. Validation is demonstrated through a series of test cases. The results indicate that the model can attain good agreement with measured data thereby demonstrating the capabilities of the multi-mode morphodynamic model system in predicting sediment-laden flows and resulting morphological change.

**Keywords:** multi-mode; morphodynamic model; bedload; suspended load; geomorphic impacts

## Introduction

Sediment transport frequently occurs in river channels, estuaries and coastal areas. In recent decades, Increasing efforts have been taken to numerical modelling of rapid sediment-laden flows and resulting morphological change (Carrivick, et al., 2010, Greimann, et al., 2008, Guan, et al., 2013, Guan, et al., 2014, Li and Duffy, 2011, Wu, 2004). In general, sediment transport is catalogued into: suspended load and bedload. The transport mechanisms of different modes differ from each other significantly. Sediment transport regime depends closely on flow properties and the type of sediment material (Soulsby, 1997). For example, bedload is rarely significant for tiny silt or fine sand; however, for gravel-bed material, bedload often takes the dominant role except in conditions of very high-energy flows. In reality, the commonly-seen mode is so-called 'mixed load' which involves suspended load and bedload dominant sheet flow. The sheet flow load is conventionally referred to as bed-load transport at high bottom shear stress for which sediment transport occurs in a layer near the bed with a thickness of several times sediment grain size (Sumer, et al., 1996).

[1*] Research Fellow, School of Civil Engineering, University of Leeds, LS2 9JT, UK. Email: Mingfu.Guan@hotmail.com
[2] Professor, School of Civil Engineering, University of Leeds, LS2 9JT, UK. Email: N.G.Wright@leeds.ac.uk
[3] Senior Lecturer, School of Civil Engineering, University of Leeds, LS2 9JT, UK. Email: P.A.Sleigh@leeds.ac.uk

To date, four types of sediment transport model have been presented in the literature. (1) The capacity model. Representative of this is the Shallow Water-Exner-based model (Benkhaldoun, et al., 2010, Diaz, et al., 2008, Murillo and Garcia-Navarro, 2010). The limitation of this approach is that the sediment transport rate is assumed to be equal at any time to the transport capacity. This method is inherently likely to cause model inaccuracy, because there are spatial and temporal lags for sediment transport to adapt to the local flow conditions (Cao, et al., 2007, Phillips and Sutherland, 1989). (2) The two-layer transport model. The initial two-layer model (Capart, 2000) assumed the velocities of the two layers to be the same and the sediment concentration in sheet flow layer to be constant. Later, the two-layer model was improved by treating the two layers separately with two groups of mass and momentum equations (Spinewine, 2005). However, the two-layer model has some limitations in that it assumes the concentration in the sheet flow layer to be constant and is rather complex in applications solving for several governing equations in two dimensions. (3) The two-phase flow model (Bakhtyar, et al., 2009, Dong and Zhang, 1999, Li, et al., 2008). The two-phase flow model is attractive for predicting sediment-laden flows and hyper-concentrated flows in open channels or coastal zones. Yet, the development of two-phase morphodynamic model are still in the infancy; and the solution time of practical sediment problems for the two-phase flow model is quite expensive even in the not-so-near future (Spasojevic and Holly, 2008). (4) The non-capacity model (Cao, et al., 2007, Capart and Young, 1998, Greimann, et al., 2008, Guan, et al., 2014, Simpson and Castelltort, 2006, Wu, et al., 2012, Wu and Wang, 2008) which is more appropriate and increasingly adopted. Yet, much room is still left to improve these models because of the limited understanding of the complex flow-sediment interactions.

Usually, suspended load is computed by an advection-reaction equation, while bedload is separately considered using an empirical bedload transport formula. Recent models have emerged to represent total sediment load in a single mode. However, it is extremely crucial to choose a modelling paradigm appropriate for the local flow conditions instead of to apply a same model to all flow-sediment events. Therefore, it is necessary to construct a flexible model system suitable for various sediment transport modes. Based on the issues outlined above, this study is directed towards presenting a multi-mode non-capacity morphodynamic model system to predict sediment-laden flows and morphological evolution. A flexible sediment transport model is presented. The model is not only applicable to bedload dominant sheet flows and suspended load dominant flows, but also suitable for the total sediment load flows. It depends on which mode is dominant in the local flow conditions. This makes the model easy to apply to complex hydraulic conditions. The model system is solved by a second-order Godunov-type finite volume method which is accurate and robust (Guan, et al., 2013). Validation is demonstrated through a series of test cases. The results indicate that the model can attain good agreement with measured data thereby demonstrating the capabilities of the multi-mode model system in predicting sediment-laden flows and resulting morphological change. Furthermore, as the sediment transport is too complex to fully understand, some empirical closure relationships or parameters are summarised and analysed for their sensitivity.

## Framework of a Multi-mode Morphodynamic Model

Based on an understanding of the physical process of flow-sediment process (Guan, et al., 2014, Spinewine and Zech, 2007), a layer-based concept divides the whole flow region into an active bed layer; a sheet flow layer and an upper suspension layer (see Fig.1). Following the shallow water theory-based non-capacity model, the model system comprises a combination of the following modules:

- *Hydrodynamic module*: it is governed by 1D shallow water equations where the flow-sediment interaction effects are accounted for as additional source terms.

- *Sediment transport module*: this module is the core of the whole model system since it decides the style of morphological evolution. A flexible sediment transport model is proposed for various sediment transport modes.

- *Morphological evolution module*: the bed elevation is updated by this model at each time step.

Sediment-laden flows are a particularly complex process; so much so that it is impossible to include all the hydraulic and sedimentary effects accurately in a model. Therefore simplifying assumptions are required. Those assumptions adopted here are: (1) non-cohesive sediment material is considered; (2) the collision effects between particles and particles are ignored; (3) the time scale of bed change is much larger than that of flow movement so that the flow is calculated assuming a "fixed" bed at each time step.
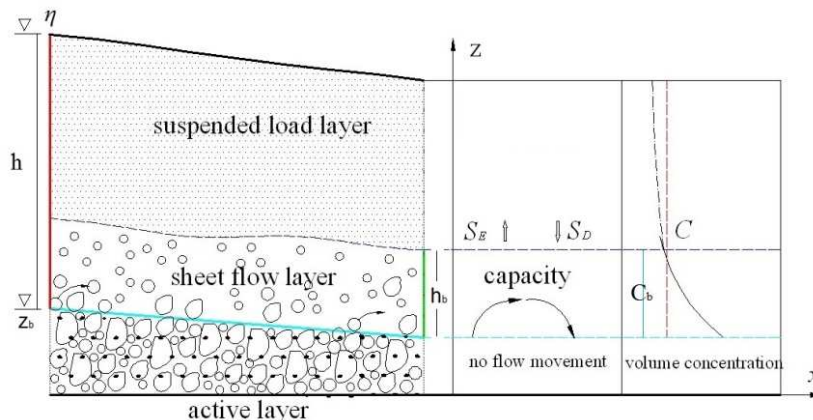


Fig.1 Schematic in the longitudinal direction with movable layer

### *Hydrodynamic Module*

The hydrodynamic model is based on the 1D shallow water equations which comprise the mass and momentum conservation equations for the water–sediment mixture flow. Coupled equations have been presented in a two-dimensional form considering the velocity different of flow and sediment by the authors (Guan, et al., 2013, Guan, et al., 2014). Following this, the modified hydrodynamic governing equations can be expressed in detail as Eq. (1) and Eq. (2). Different from the traditional shallow water equations, the hydrodynamic governing equations incorporate the sediment transport effects by involving the mass and momentum exchange between flow phase and sediment phase as additional source terms (Guan, et al., 2014).

$$\frac{\partial \eta}{\partial t} + \frac{\partial hu}{\partial x} = 0 \tag{1}$$

$$\frac{\partial hu}{\partial t} + \frac{\partial}{\partial x}\left(hu^2 + \frac{1}{2}gh^2\right) = gh(S_o - S_f) + \frac{\Delta\rho u}{\rho}\frac{\partial z_b}{\partial t}[\xi(1-p) - C] - \frac{\Delta\rho gh^2}{2\rho}\frac{\partial C}{\partial x} - S_A \tag{2}$$

$$S_A = (1 - \xi)\frac{\Delta\rho u}{\rho}\left(C\frac{\partial hu}{\partial x} - hu\frac{\partial C}{\partial x}\right)$$

where $t$ = time; $x$ = longitudinal coordinate; g = gravity acceleration (m/s²); $\eta$ = water surface elevation (m); $z_b$ = bed elevation (m); $h = \eta\text{-}z_b$ = flow depth (m); $u$ = depth-averaged flow velocity (m/s); $\Delta\rho = \rho_s\text{-}\rho_w$ = the difference of sediment density and water density (kg/m³); $p$ is the sediment porosity (dimensionless); $C$ = total volumetric concentration in whole flow depth (dimensionless); $\rho = \rho_w(1\text{-}C)+\rho_s C$ = density of sediment-water mixture (kg/m³); $S_o$ = bed slope (dimensionless); $S_f$ = friction slope which is determined from Manning's equation here. $\xi$ = the sediment-to-flow velocity coefficient; $S_A$ = additional momentum transfer term related to the velocity difference between sediment and flow.

### *Sediment Transport Module*

This module involves three sediment transport models (denoted as STM in the following). STM1 presents a bedload dominant sheet flow model considering the velocity difference of flow and sediment; STM2 introduces a suspended load model. By combining STM1 with STM2, a flexible sediment transport model STM3 is proposed with the incorporation of a weight coefficient of bedload and suspended load.

**STM1: Bedload Dominant Sheet Flow Model**

The governing equations of sheet flow model is derived based on the mass conservation equation of sediment in sheet flow layer (Singh, 1996, Wu, 2004). It is written by

$$\frac{\partial h_b C_b}{\partial t} + \frac{\partial h_b u_b C_b}{\partial x} = -\frac{(q_b - q_{b*})}{L} \tag{3}$$

where $h_b$ = the thickness of the sheet flow layer (m); $u_b$ = sheet flow velocity (m/s); $C_b$ = volumetric sediment concentration in sheet flow layer (dimensionless); $q_b$ = sediment transport rate (m²/s); $q_{b*}$ = sediment transport capacity (m²/s); $L$ = non-equilibrium adaptation length of sediment transport (m).

In order to readily solve the hydrodynamic model and sediment transport model, the $h_b$, $u_b$, $C_b$ for the sheet flow layer are replaced by $h$, $u$, and a volumetric bedload concentration $S_b$ in the whole flow depth as $h_b u_b C_b = huS_b \rightarrow h_b C_b = u/u_b hS_b = \beta hS_b$ where $\beta = u/u_b$ is the flow-to-sediment velocity ratio. The above relationship is substituted into Eq. (3) which is then expanded. Eq. (3) is approximately replaced by

$$\frac{\partial hS_b}{\partial t} + \frac{1}{\beta}\frac{\partial huS_b}{\partial x} = -\frac{1}{\beta}\frac{(q_b - q_{b*})}{L} \tag{4}$$

The flow-to-sediment velocity ratio has been widely studied and formulated by previous research (Greimann, et al., 2008, van Rijn, 1984). In this paper, Eq. (5) proposed by Greimann, et al., (2008) is used to estimate the approximate velocity ratio for weak sediment transport; for the severe sediment transport, we assume the

sediment and flow velocity to be approximately equivalent. Furthermore, the non-equilibrium adaptation length $L$ has been investigated by many researchers (Armanini and Di Silvio, 1988, Greimann, et al., 2008, Phillips and Sutherland, 1989, Wu, 2004), but still warrants further study. Here, following the previous research, $L$ is calculated by Eq. (6).

$$\frac{1}{\beta} = \frac{u_b}{u} = \frac{u_*}{u} \frac{1.1(\theta/\theta_{cr})^{0.17}[1 - e^{-5\theta/\theta_{cr}}]}{\sqrt{\theta_{cr}}} \qquad (5)$$

$$L = \frac{hu}{\gamma \omega_0} \qquad (6)$$

where $\theta$, $\theta_{cr}$ are the real dimensionless bed shear stress and the critical dimensionless bed shear stress (dimensionless); $u_* = \sqrt{ghS_f}$ represents the shear velocity; $\omega_0$ is the effective settling velocity of sediment particles (m/s), which is estimated by van Rijn's equation (van Rijn, 1984); $\gamma$ is an empirical dimensionless coefficient proposed by several authors (Armanini and Di Silvio, 1988, Greimann, et al., 2008, Wu, 2004). For sheet flow in this paper, $\gamma$ is regarded as the ratio of the near-bed concentration and the volumetric concentration in flow. As the near-bed concentration must not be larger than ($1-p$), $\gamma$ is calculated as

$$\gamma = \min\left(\frac{C_b}{S_b}, \frac{1-p}{C}\right) = \min\left(\frac{u}{u_b}\frac{h}{h_b}, \frac{1-p}{C}\right) = \min\left(\frac{1}{\beta}\frac{h}{h_b}, \frac{1-p}{C}\right) \qquad (7)$$

The thickness of the sheet-flow layer is calculated by the relationship $h_b = \mu\theta d_{50}$ (Jenkins and Hanes, 1998, Pugh and Wilson, 1999, Sumer, et al., 1996), where $\mu$ is a dimensionless coefficient. For bedload transport equations, a commonly-used relationship is Meyer-Peter & Müller equation (Meyer-Peter and Müller, 1948) (denoted as MPM in the following). Yet, the application ranges of the MPM equation are: bedload transport; bed slope from 0.0004 to 0.02 and Shields number of < 0.25 (Meyer-Peter and Müller, 1948). Therefore, it might be open to question for applications to outburst flow or cases with steeply sloped beds. Thus, a calibration coefficient $\psi$ is suggested in the original MPM equation giving:

$$q_{b*} = \psi 8(\theta - \theta_{cr})^{1.5}\sqrt{(\rho_s/\rho_w - 1)gd_{50}^3} \qquad (8)$$

For a bed slope of ≥0.03, Smart and Jäggi (Smart and Jäggi, 1983) (denoted as SJ in the following) expanded the database obtained by Meyer-Peter & Müller (Meyer-Peter and Müller, 1948) for the steep slope of 0.03-0.20. They performed flume experiments to estimate the transport capacity of mountain streams. For bed slope>0.2, in this paper we make the approximation of assuming the maximum bed slope $S_{max}$ to be 0.2 in the equation to avoid the calculated transport rate becoming un-physically large due to exceeding the bed slope limit. The slightly modified equation is written by:

$$q_{b*} = 4\left(\frac{d_{90}}{d_{30}}\right)^{0.2}\frac{h^{1/6}}{n\sqrt{g}}\min(S_o, 0.2)^{0.6}\theta^{0.5}(\theta - \theta_{cr})\sqrt{(\rho_s/\rho_w - 1)gd_{50}^3} \qquad (9)$$

where $d_{30}$, $d_{50}$, and $d_{90}$ are the 30th, 50th, and 90th percentile grain size, respectively; $n$ is Manning's roughness ($m^{1/3}$/s).

**STM2: Suspended Load Transport**

At high bed shear stress, fine sediment particles can be easily entrained into suspension if the lift force exceeds the grain weight or the bed shear stress exceeds the critical value, e.g. suspension occurs for silt or very fine sand, and for relatively coarse sand under the condition of high-energy outburst flows. In this regard, suspended load transport is governed by simplified advection-diffusion equation as:

$$\frac{\partial hS}{\partial t} + \frac{\partial huS}{\partial x} = S_E - S_D \tag{10}$$

where $S$ = volumetric suspended load concentration; $S_E$ = entrainment flux of sediment; $S_D$ = deposition flux of sediment. For suspended load dominant transport, the entrainment flux and deposition flux of sediment are vital; however, there is no a universal theoretical expression for these. Both $S_E$ and $S_D$ are calculated by the empirical functions. The interface between the sheet flow layer and suspended-load layer is assumed to be at a reference level $a$, then the deposition flux is represented as a product of the effective sediment settling velocity and the near-bed concentration at the reference level: $S_D = \omega_0 C_a$. Therein $C_a = \delta S$ is the near-bed concentration at the reference level $a$. The definition of coefficient $\delta$ by Cao et al. (2004) is used here: $\delta = \min\{2.0, (1 - p)/C\}$. The entrainment flux of sediment is calculated by $S_E = \omega_0 C_{ae}$, where $C_{ae}$ is the near bed equilibrium concentration at the reference level determined by using the function of van Rijn (1984).

$$C_{ae} = 0.015 \frac{d_{50}}{a} \frac{T^{1.5}}{d_*^{0.3}} \tag{11}$$

$$T = \frac{(u_*^2 - u_{*,cr}^2)}{u_{*,cr}^2}$$

$$a = \min[\max(k_s, 2d_{50}, 0.01h), 0.2h]$$

where $k_s$ is the equivalent roughness height; $d_* = d_{50}[(\rho_s/\rho_w-1)g/\nu^2]^{1/3}$ is the dimensionless particle diameter; $\nu$ is the viscosity of water; $u_*' = u(\sqrt{g}/C')$ is bed-shear velocity related to grain; $C'$ is the Chézy-coefficient related to grain; $u_{*,cr}$ is the critical bed-shear velocity.

**STM3: Flexible Sediment Transport Mode**

Based on STM1 and STM2 presented above, a flexible sediment transport equation is formulated by combining Eq.(4) and Eq.(10) and incorporating a weight coefficient into them as:

$$\frac{\partial hC}{\partial t} + \xi \frac{\partial huC}{\partial x} = -\alpha \frac{1}{\beta} \frac{(q_b - q_{b*})}{L} + (1 - \alpha)(S_E - S_D) \tag{12}$$

where $\xi = \alpha \frac{1}{\beta} + (1 - \alpha)$ represents sediment-to-flow velocity coefficient for total sediment transport; $\alpha$ denotes a weight coefficient of bedload transport in total load; here $\alpha$ is defined as 1 for bedload dominant sheet flow model, $\alpha$ is equal to 0 for suspended load model, and $\alpha=[0,1]$ is used for fully suspended load and bedload model. The weight coefficient $\alpha$ specifies how much of a sediment size class is transported as bed load, suspended load, or mixed load. In physical sense, it is difficult to distinguish suspended load and bed load from each other where both coexist. However, some research (Greimann, et al., 2008, van Rijn, 1984)

indicated $\alpha$ to be primarily a function of the suspension parameter. To estimate the weighting coefficient governing the relative importance of bedload and suspended load transport, the following equation proposed by Greimann et al. (2008) is used in this study:

$$\alpha = 1 - \min(1, 2.5e^{-Z}) \tag{13}$$

where $Z = \omega_f/(\kappa u_*)$, $\kappa = 0.41$ = von Kármán constant..

### *Morphological Evolution Module*

The purpose of this module is to update the new bed elevation on the basis of the results from the calculation of the previous two modules. The bed erosion and deposition is calculated per grid cell at each time step by the following equation:

$$\frac{\partial z_b}{\partial t} = \frac{1}{(1-p)}\left[\alpha \frac{(q_b - q_{b*})}{L} + (1-\alpha)(S_D - S_E)\right] \tag{14}$$

### *Bed Slope Effects*

One of the most important influences of bed slope is its effect on the critical shear stress for initial sediment motion. A number of studies have highlighted that the variation in channel gradient has an influence over the mean bed shear stress at which sediment is entrained (Lamb, et al., 2008, Parker, et al., 2011). For the threshold of sediment motion, the empirical Eqn. (Soulsby, 1997) is applied here,

$$\theta_c = \frac{0.30}{1 + 1.2d_*} + 0.055[1 - e^{-0.02d_*}] \tag{15}$$

Based on the study of Smart and Jäggi (Smart and Jäggi, 1983); the revised critical dimensionless bed shear stress is determined according to the relation of flow and slope direction as:

$$\theta_{cr} = \theta_c \begin{cases} \cos(\arctan |S_o|)(1 - |S_o|/\tan\varphi) & for \ u \cdot S_o < 0 \\ \cos(\arctan |S_o|)(1 + |S_o|/\tan\varphi) & for \ u \cdot S_o > 0 \end{cases} \tag{16}$$

where $\theta_{cr}$ is a corrected critical Shields parameter for high slopes, $\varphi$ is the sediment angle of repose.

### *Unstable Bed Slope Collapse*

If the slope angle of a non-cohesive bed becomes larger than the critical angle of bed slope, the bed material will slide or avalanche to form a new slope approximately equal to the critical value. The process of avalanching is simulated by enforcing $|\varphi_i| < \varphi$, while maintaining the mass continuity between adjacent cells. The update equation for the re-deformed bed level is derived as follows: when $\varphi_i > \varphi$, the new bed slope angle

is set approximately equal to be the angle of repose by lowering the higher elevation cell and elevating the lower elevation cell. Therefore, the bathymetry is modified as

$$\begin{cases} z_{new,i+1} = z_{i+1} - \Delta z_x \\ z_{new,i} = z_i + \Delta z_x \end{cases} \tag{17}$$

where $\Delta z_x = \begin{cases} \frac{\Delta z}{2} \approx \text{sign}(\varphi_i)\frac{dx_i(\tan|\varphi_i|-\tan\varphi)}{2} & |\varphi_i| > \varphi \\ 0 & |\varphi_i| \le \varphi \end{cases}$ with $\text{sign}(\varphi_i) = \begin{cases} 1 & \varphi_i > 0 \\ 0 & \varphi_i = 0 \\ -1 & \varphi_i < 0 \end{cases}$

Since avalanching between two adjacent cells may induce new avalanching at neighbouring cells, the sweeping process is repeated by use of Eq. (17) until no avalanching occurs.

## Numerical Solution

Eqs.(1), (2) and (12) constitute a non-linear hyperbolic system. Currently, a range of numerical schemes has been proposed and can be utilised to solve such hyperbolic system. Here a second-order upwind Godunov-type scheme with a HLL Approximate Riemann Solver is applied to solve the coupled model (Guan, et al., 2013). The governing equations are rewritten in compact form as follows

$$\frac{\partial \mathbf{U}}{\partial t} + \frac{\partial \mathbf{F}}{\partial x} = \mathbf{S} \tag{18}$$

where $\mathbf{U}$ = the vector of the conservative variables; $\mathbf{F}$ = the flux vector which is the function of conservative variables; $\mathbf{S}$ = the vector of source terms

$$\mathbf{U} = \begin{bmatrix} \eta \\ hu \\ hC \end{bmatrix}; \ \mathbf{F} = \begin{bmatrix} hu \\ hu^2 + \frac{1}{2}gh^2 \\ \xi huC \end{bmatrix}; \ \mathbf{S} = \begin{bmatrix} 0 \\ gh(S_o - S_f) + \frac{\Delta\rho u}{\rho}\frac{\partial z_b}{\partial t}[\xi(1-p) - C] - \frac{\Delta\rho gh^2}{2\rho}\frac{\partial C}{\partial x} - S_A \\ -\alpha\frac{1}{\beta}\frac{(q_b - q_{b*})}{L} + (1-\alpha)(S_E - S_D) \end{bmatrix}$$

With respect to discretisation of conservative variables, the shallow water equations are discretised conservatively by using the finite volume method (FVM).

$$\mathbf{U}_i^{n+1} = \mathbf{U}_i^n - \frac{\Delta t}{\Delta x}\left(\mathbf{F}_{i+1/2}^* - \mathbf{F}_{i-1/2}^*\right) + \Delta t \mathbf{S}_i \tag{19}$$

The interface flux between the two neighbouring cells is calculated by the HLL scheme expression as follows:

$$\mathbf{F}_{i+1/2}^* = \begin{cases} \mathbf{F}_i & if \ S_L \ge 0 \\ \mathbf{F}_{i+1} & if \ S_R \le 0 \\ \mathbf{F}^* & otherwise \end{cases} \tag{20}$$

where $\mathbf{F}_i = \mathbf{F}(\mathbf{U}_i)$, $\mathbf{F}_{i+1} = \mathbf{F}(\mathbf{U}_{i+1})$ are the flux and conservative variable vectors at the left and right sides of each cell interface; the $S_L$, $S_R$ denote two wave speeds which must be selected carefully to avoid any entropy violation; $\mathbf{F}^*$ is the numerical flux in the star region, calculated in two dimensions by

$$\mathbf{F}^* = \frac{S_R\mathbf{F}_i - S_L\mathbf{F}_{i+1} + S_R S_L(\mathbf{U}_{i+1} - \mathbf{U}_i)}{S_R - S_L} \tag{21}$$

The $S_L$ and $S_R$ are estimated by the so-called "two expansion" including dry-bed options. They are expressed by

$$S_L = \begin{cases} \min\left(u_i - \sqrt{gh_i}, u^* - \sqrt{gh^*}\right) & if\ h_i > 0 \\ u_{i+1} - 2\sqrt{gh_{i+1}} & if\ h_i = 0 \end{cases} \tag{22a}$$

$$S_R = \begin{cases} \min\left(u_{i+1} + \sqrt{gh_{i+1}}, u^* - \sqrt{gh^*}\right) & if\ h_{i+1} > 0 \\ u_i + 2\sqrt{gh_i} & if\ h_{i+1} = 0 \end{cases} \tag{22b}$$

where $u^* = \frac{1}{2}(u_i + u_{i+1}) + \sqrt{gh_i} - \sqrt{gh_{i+1}}$; $\sqrt{gh^*} = \frac{1}{2}\left(\sqrt{gh_i} + \sqrt{gh_{i+1}}\right) + \frac{1}{4}(u_i - u_{i+1})$

To calculate the inter-cell numerical fluxes, a weighted average flux (WAF) total variation diminishing (TVD) method is employed with a flux limiter function.

$$\mathbf{F}_{i+1/2}^* = \frac{1}{2}(\mathbf{F}_i + \mathbf{F}_{i+1}) - \frac{1}{2}\sum_{k=1}^{N} sign(c_k)\Phi_{i+1/2}^k \Delta\mathbf{F}_{i+1/2}^k \tag{23}$$

where $c_k$ is the Courant number for wave $k$, $c_k = \Delta t S_k/\Delta x$; $S_k$ is the speed of wave $k$ and $N$ is the number of waves in the solution of the Riemann problem. $N = 2$ when applied in conjunction with the HLL approximate Riemann solver. $\Delta\mathbf{F}^{(k)}_{i+1/2} = \mathbf{F}^{(k+1)}_{i+1/2} - \mathbf{F}^{(k)}_{i+1/2}$, which is the flux jump across wave $k$; $\mathbf{F}^{(k)}_{i+1/2}$ is the value of the flux vector in the interval $k$; herein $\mathbf{F}^{(1)}_{i+1/2} = \mathbf{F}(\mathbf{U}_L)$, $\mathbf{F}^{(2)}_{i+1/2} = \mathbf{F}(\mathbf{U}^*)$, and $\mathbf{F}^{(3)}_{i+1/2} = \mathbf{F}(\mathbf{U}_R)$ which are estimated by the HLL approximate Riemann solver, $\Phi(r)$ is the WAF limiter function. The WAF limiter used here is the *minmod* limiter expressed by $\varphi(r)$:

$$\Phi(r) = 1 - (1-|c|)\varphi(r) \text{ with } \varphi(r) = \max[0, \min(1, r)] \quad (minmod\ limiter) \tag{24}$$

where $r^{(k)}$ is the ratio of the upwind change to the local change in scalar quantity $q$. It can be written by:

$$r^{(k)} = \begin{cases} \Delta q_{i-\frac{1}{2}}^{(k)} \Big/ \Delta q_{i+\frac{1}{2}}^{(k)} = \left(q_i^{(k)} - q_{i-1}^{(k)}\right) \Big/ \left(q_{i+1}^{(k)} - q_i^{(k)}\right) & if\ c_k > 0 \\ \Delta q_{i-\frac{3}{2}}^{(k)} \Big/ \Delta q_{i+\frac{1}{2}}^{(k)} = \left(q_{i+2}^{(k)} - q_{i+1}^{(k)}\right) \Big/ \left(q_{i+1}^{(k)} - q_i^{(k)}\right) & if\ c_k > 0 \end{cases} \tag{25}$$

We choose $q = \eta$ (water surface elevation) for the left wave $S_L(k = 1)$ and the right wave $S_R(k = 2)$. For the bed slope source term treatment, the homogenous flux approach is applied here (Guan, et al., 2013, Lee and Wright, 2010). The computation procedure at each time step can be described as:

(1) to input initial hydraulic and sediment information, including flow depth, flow velocity, sediment concentration and bed elevation;

(2) to calculate the dimensionless bed shear stress using the information from step (1);

(3) to estimate the weight coefficient of bedload transport using Eq. (13);

(4) to calculate the bedload transport capacity according to the empirical functions and the entrainment/deposition fluxes of suspended load;

9

(5) to solve the model system of Eqs. (1), (2), (12) based on the information from above-steps and to update the hydraulic and sediment information;

(6) to update the bed elevation calculated by Eq. (14) ;

(7) to evaluate the stability of the newly formed bed by Eq. (17);

(8) to return the step (1) and repeat step (1) to (6).

A variable time step $\Delta t$, adapted to hydraulic parameters variability, is calculated by the following equation. As the numerical scheme is explicit, the restriction of Courant number $0<CFL<1.0$ is implemented for the solution of the coupled model.

$$\Delta t = CFL \min \frac{\Delta x_i}{|u_i|+\sqrt{gh_i}} \tag{26}$$

At the wetting and drying front, small water depths can cause unrealistically high velocity, which in turn causes numerical instabilities. To overcome this, we introduced a water depth tolerance. If the water depth is smaller than the tolerance depth, it will be treated as a dry bed case whose velocity is set equal to zero; otherwise, it is treated as a wet bed case. Furthermore, updating the water depth at each time step may cause a negative value to occur, which violates mass conservation and will lead to a gain of mass. Thus, a special treatment method introduced in (Guan, et al., 2013) was used to maintain mass conservation of the numerical solution. A detailed description can be found in our study (Guan, et al., 2013).

## Numerical Tests

A range of test cases are considered in order to test various aspects of the proposed model system.

### *Sediment Transport in a Trench*

This test is to verify the capability of the proposed model to predict bed evolution under the conditions of unsteady flows. The experiments were originally conducted at the Delft Hydraulics Laboratory to investigate the movable bed evolution caused by steady open channel flow. Three tests with different side slopes of 1:3, 1:7 and 1:10 were performed in the experiments. One of them, Test 3 with a side slope of 1:10 was reproduced by the model. Fig.2 illustrates the initial configurations of the trench profiles of Test 3. The mean inflow velocity was 0.51 m/s at the inlet and the water depth were kept constant as 0.39 m. The erodible bed is constituted by fine sand with $d_{10} = 0.115$ mm, $d_{50} = 0.16$ mm and $d_{90} = 0.2$ mm. The sand density and porosity was 2,650 kg/m$^3$ and 0.4 respectively. According to the experiment, the settling velocity of sediment particle was 0.013 m/s ± 25%. The hindering setting velocity $\omega_0 = 0.015$ m/s is used. Manning's coefficient $n$ is set to be 0.016. In addition, to maintain the sediment equilibrium conditions in the upstream, i.e. no scour or deposition occurs, sand with the same composition was fed at a constant rate of 0.04 kg/s/m; therein, the suspended load transport rate was estimated to be 0.03 ± 0.006 kg/s/m and the bed load transport rate of about 0.01 kg/s/m.
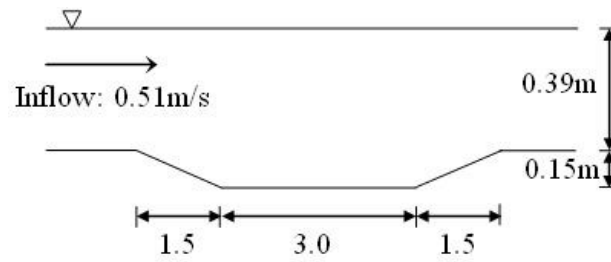
Fig.2 Initial experimental setup

For simulation, the whole domain is discretised by 150 cells with $\Delta x = 0.2$ m. To make the flow to be steady flow, the model is run in 900 s, keeping bed profile to be unchanged. After 900 s, sand is fed and bed evolution occurs. Van Rijn (1984) suggested the reference level to be estimated using the following equation, $a = \min[\max(k_s, 2d_{50}, 0.01h), 0.2h]$. Based on this formulation, $a = 0.01$ m was calibrated to be good for maintaining the sediment equilibrium in upstream of the channel. To show the influence of the reference level $a$, a sensitivity test was implemented with the inputs of $a = 0.005$ m, $a = 0.01$ m and $a = 0.02$ m. Fig. 3 indicates that the bed profiles are slightly influenced by the reference level at t = 7.5 h, however, $a = 0.005$ m over-predicts the bed evolution remarkably at t = 15 h, but $a = 0.01$ m and $a = 0.02$ m simulate similar bed profiles with a slight difference. It is clear that the smallest reference level leads to the fastest bed change, because in the steady event, a larger entrainment flux due to a smaller reference level must increase the corresponding near-bed concentration in order to maintain the steady state, which accelerates the bed evolution. Also, the empirical reference level proposed by van Rijn (1984) has an empirical constraint, $a = 0.005$ m probably causes an unreasonable estimation on the near-bed equilibrium sediment concentration using Eq. (11). Considering the equilibrium of upstream channel, the calibrated value $a = 0.01$ m was used here. The measurement indicated that the contribution of suspended load to total load was in a range of 60% - 90%, so an average weight coefficient $\alpha = 0.25$ and Eq. (13) were used to verify how the flexible sediment transport model performs. As shown in Fig. 4(a)(b), it can be seen that very similar bed profiles were predicted by using the two estimated weighting coefficients. Fig. 4(c) demonstrates the portions of suspended load along with the channel at t = 7.5 h and 15 h respectively. The predicted portion of suspended load is mostly in range of 60% - 80%, which fits the measured range fairly well. In addition, two other runs with a finer mesh $\Delta x = 0.1$ m and a coarser mesh $\Delta x = 0.3$ m was conducted to verify the influence of mesh size on the simulation bed change. Fig. 5 shows that slight differences are observed for the different mesh resolution and the finer mesh predicts a slight deeper upstream slope and deeper scour hole. Overall, the influence of mesh size is not so significant. The solution appears to be convergent. This reveals that the flexible model can predict the morphological evolution effectively caused by sediment-laden flow with both suspended load and bedload.
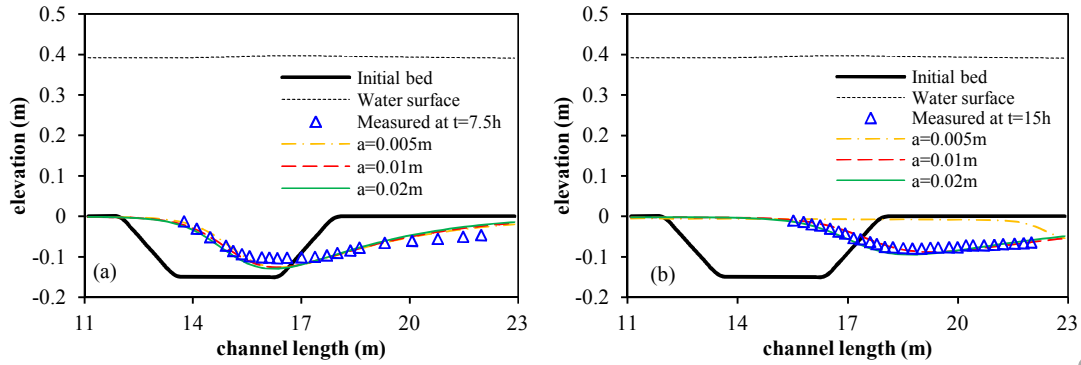
11

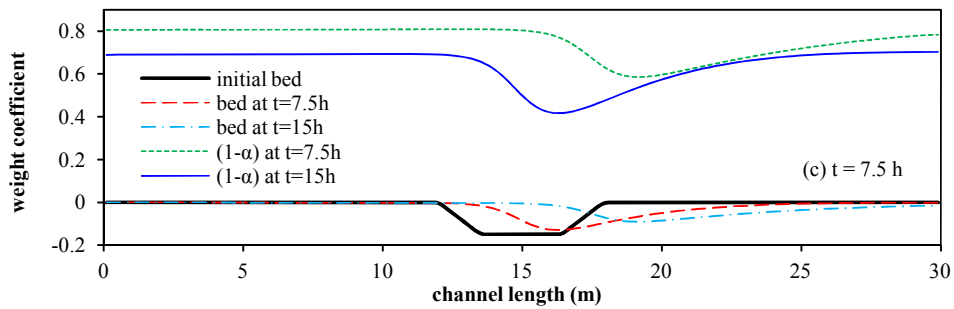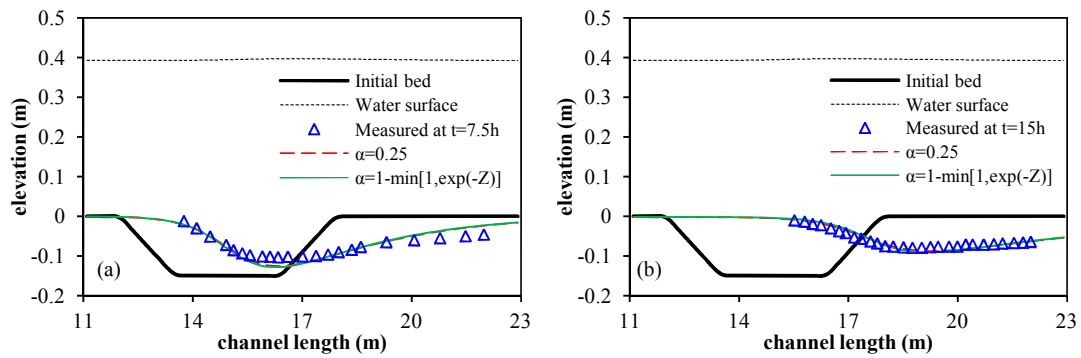Fig.3 Simulation results for different reference level at 7.5 h and 15 h



Fig.4 Simulation results for different weighting coefficient at (a) 7.5 h and (b) 15 h, (c) weighting coefficient along with the channel at 7.5 h and 15 h
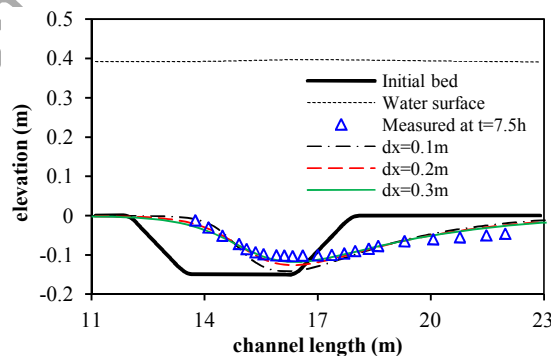


Fig.5 Simulation results for different mesh sizes

### Dam-break Flow over a Movable Bed

In this section, the erosion and deposition processes induced by unsteady outburst flow are reproduced in order to validate the applicability of the proposed model. A sand bed and a bed of PVC particles are tested and the simulated results are compared with the measured data. Bedload is the main mode for both tests, thus the weight coefficient $\alpha=1$ is used here.

12

**Sand Bed**

Dam-break flow over movable bed experiments were conducted in the laboratory of the Civil and Environmental Engineering Department at UCL in Belgium (Spinewine, 2005, Spinewine and Zech, 2007). A horizontal glass-walled flume of 6 m × 0.25 m × 0.70 m rectangular cross-section was used. A thin gate was located at the middle of the flume. The bed material was water-saturated sand with a diameter of 1.82 mm, density of 2,683 kg/m³, porosity of 0.47 and repose angle of 30°. Different initial conditions were tested by adjusting the initial water depth and the thickness of movable bed upstream and downstream of the gate. In this test, three configurations are simulated. The first one is a dam-break flow over a flat bed with a thickness of 0.125 m for the movable bed, and the water depths before and after the gate are 0.35 m and 0 m respectively. The second and third configurations consider a dam-break over a movable bed with a downward bed step of 0.1 m and upstream water depth of 0.25 m. Downstream water depth for the second configuration is 0 m and for the third configuration it is 0.10 m.

The channel is discretised with 600 cells ($\Delta x$ = 0.01 m); the Manning's coefficient is set as 0.018 in line with the experimental work. Simulations with and without the inclusion of bed slope avalanching are carried out in order to explain the role the unstable bed avalanching plays in the morphodynamic model. The simulated results at t = 6.6 $t_0$ are shown in Fig. 6, where $t_0$ = 0.189 s and $H_0$ = 0.35 m. The simulated water surfaces and bed profiles are compared with measured data in Fig. 6. The comparisons show that the three key factors, water front, water surface and bed level, are predicted effectively with the inclusion of bed slope avalanching and the simulated results agree well with the measured results. Secondly, from the results with and without the inclusion of bed slope avalanching, we can conclude that the reformation of the unstable bed is necessary when carrying out morphodynamic modelling work. A similar verification on the necessity of slope stability operator has been verified by the study of (Zech, et al., 2008). As demonstrated in Fig. 6 (b, c), both simulated water surface and bed profile without bed slope avalanching are predicted poorly at the vertical step. Finally, there are some small discrepancies in water surfaces and bed change. This is likely to be due to uncertain empirical parameters and energy loss in the experimental case not captured in the model. In summary, the avalanching of an unstable bed slope is vital in a morphodynamic model, the simulated results with the inclusion of bed slope avalanching are acceptable and satisfactory; and the proposed model predicts the morphological process induced by outburst flow with good agreement.
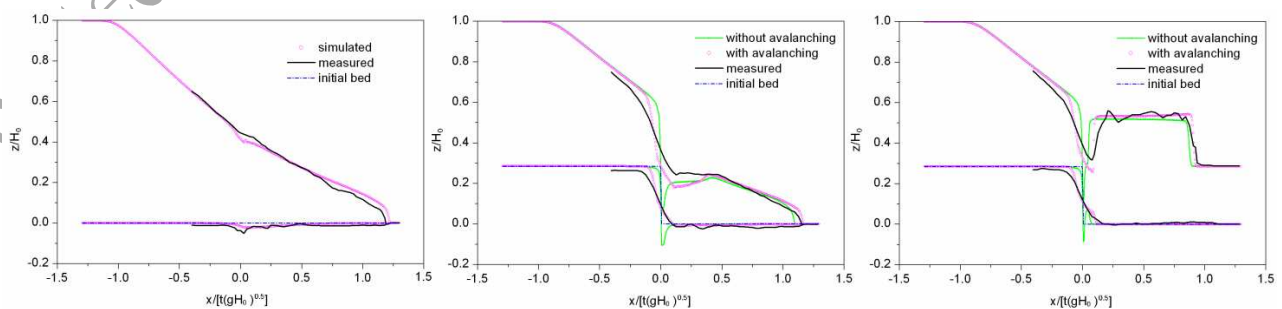


Fig.6 Comparison between the simulated results and experimental data at t = 6.6 $t_0$ for the three configurations; (a) no bed step, the downstream is dry, (b) the height of bed step is 0.1 m, the downstream is dry, and (c) the height of bed step is 0.1 m, the downstream depth is 0.1 m

**PVC Particles**

In this experiment, also carried out at UCL (Fraccarollo and Capart, 2002), the sediment particles were cylindrical PVC pellets having an equivalent spherical diameter of 3.5 mm, density of 1,540 kg/m$^3$ and settling velocity of about 18 cm/s. The experiments were performed in a horizontal prismatic flume with a rectangular cross section of 2.5 m × 0.1 m × 0.25 m. In this test, bedload is the dominant mode of sediment transport. For the simulation the sediment porosity is taken as 0.47. For this test case the 1D solver is used and the computational area is discretised with 200 cells in one dimension ($\Delta x$ = 0.0125 m). The experiment was run for 2 s. When the gate is removed, the water front moves rapidly downstream and erodes the bed progressively. A hydraulic jump occurs at the location of the gate where the maximum eroded depth is generated. Fig. 7(a-c) plots the simulated and measured bed profiles and water surfaces, as well as the calculated adaptation length L using Eq. (6) at three stages. It is seen that (1) the trend of water surfaces and bed profiles agree well with the measured data; (2) the maximum eroded depth of bed is simulated well; and (3) the adaptation length of sediment varies with the flow conditions, and the maximum occurs near the water front; (4) the hydraulic jump is numerically observed; although there is a discrepancy in terms of quantitative comparisons as shown in many studies with different types of models (Wu and Wang 2007, Benkhaldoun et al. 2010, Shakibaeinia and Jin 2011), this test shows that the model can address rapid transient bed deformation with good results. Adaptation length of sediment is generally subject to uncertainty. The method used in this study considered it to be a function of water depth and flow velocity. A relationship of adaptation length and shear velocity for this case is shown in Fig. 7(d). It is clear that adaptation length of sediment has a second-order polynomial relationship with shear velocity ($R^2$ > 0.97), but the relationships behind the waterfront and in the waterfront is clearly different. The value with a same shear velocity in the waterfront is smaller than that behind the waterfront.
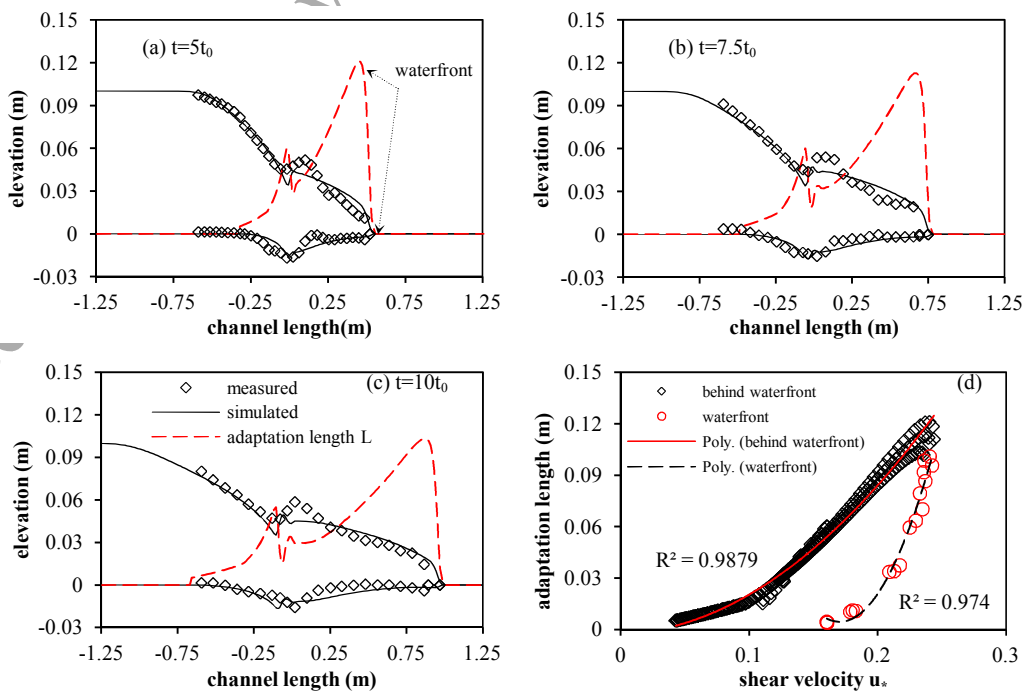
Fig.7 The simulated and measured bed profiles and water surfaces, as well as the value of adaptation length *L*; (a) t = 5 $t_0$, (b) t=7.5$t_0$, (c) t = 10 $t_0$ ($t_0$=0.101s), and (d) the relationship of adaptation length and shear velocity

*Sediment Aggradation under Transcritical Flow*

To test the methodology further it is necessary to consider the deposition of particles. Experiments on wedge aggradation caused by sediment overloading have been performed at the St. Anthony Falls Laboratory by Seal et al. (Seal, et al., 1997). Compared to the test in Section 4.2, this test is not under conditions of rapid outburst flow and the sediment deposition takes a more important role during the entire experiment. Therefore, this test is considered in order to verify that the model can represent sediment transport in transcritical flow and predict sediment deposition effectively. Run1 from the experiment is reproduced with the model (see Fig. 8). The experiment was conducted in a rectangular channel of 45 m × 0.305 m, with an initial bed slope of 0.002; the inflow discharge was a constant as 0.049 m³/s with a sediment feed rate of 0.19 kg/s at 1 m downstream of the head gate of the flume. To obtain transcritical flow over the wedge, the tailgate was kept at a constant height as 0.4 m so that a hydraulic jump or a shock wave was produced at the downstream end of the main gravel deposit. The material fed in was a gravel and sand mixture comprising a wide range of sizes from 0.125 to 64 mm and $d_{50}$ = 6 mm; the mixture porosity is 0.3. In line with the experiment, the Manning's coefficient is set as 0.028 m$^{1/3}$/s and the angle of repose is 32°. Bedload is the dominant mode, thus the weight coefficient $\alpha$ = 1 is used.
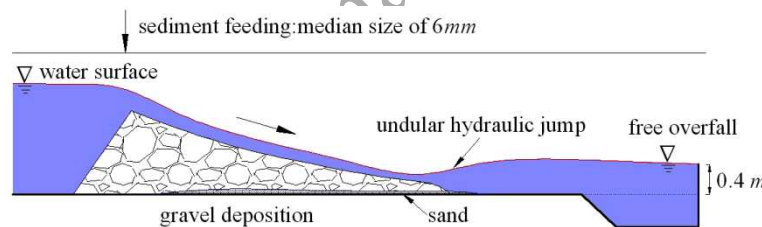


Fig.8 Schematic of the experimental setup of Seal et al. (1995)

The computational model is run for 16.8 hours of simulated time. In this case, a hydraulic jump occurs at the wedge front and a steeper bed slope is formed. Fig. 9 shows the comparisons between the measured and predicted bed profiles at t = 2 h, 8 h and 16.8 h, as well as a comparison of the water surface at t = 16.8 h. It can be seen that the simulated beds and water surfaces agree very well with the measured results, particularly in the early stages; but the simulated bed and water surface profiles at 16.8 h are slightly higher than the measured results. This is likely to be due to the particles-particles collision effects and momentum losses in the experiment which are neglected by the numerical model; also, the uncertain empirical parameters can cause errors. However, overall, it is clearly shown that the proposed model is capable of predicting the sediment deposition with good agreement and capturing of the hydrodynamic and morphodynamic characteristics in the case of sediment transport under transcritical flow.
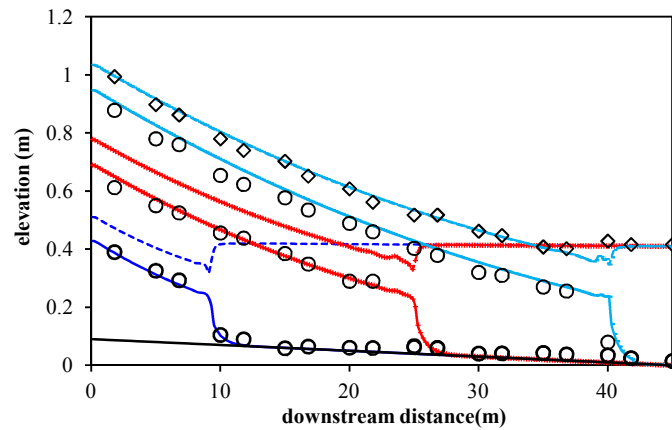
Fig.9 Comparisons between the simulated results and measured results; where circles are the measured bed; rectangular marker is the water surface at t=16.8hr; solid lines are the simulated bed; dash lines are the simulated water surface

## Dyke Erosion due to Flow Overtopping

Dyke erosion due to flow overtopping is a complex flow process involving outburst flow, supercritical flow, subcritical flow and steady flow. Further, in this situation bed slope effects occur due to the existence of upstream and downstream slopes. Additionally, it is also important to predict the flow propagation and dyke erosion processes to inform risk management. Therefore, this test is undertaken to verify that the proposed model system can solve this sediment transport problem under complex hydraulic conditions while at the same time predicting the morphological change. Here we reproduce experimental Run2 of Chinnarasri et al. (Chinnarasri, et al., 2003). A dyke was located in the middle of a flume of 35 m × 1 m × 1 m being 0.8 m in height, 1 m wide with a crest width of 0.3 m (see Fig.10). The upstream and downstream slope of the dam was 1V:3H and 1V:2.5H, respectively. The dyke is composed of sand with a median diameter of 1.13 mm, $d_{30} = 0.52$ mm, $d_{50} = 0.86$ mm, $d_{90} = 3.8$ mm and the density of $2.65 \times 10^3$ kg/m$^3$. The initial reservoir level is 0.83 m and the downstream water level is 0.03 m; the inflow discharge has a constant value of $1.42 \times 10^{-3}$ m$^3$/s; the bed material porosity is taken as 0.35. The weight coefficient of bedload is estimated by Eq. (13).
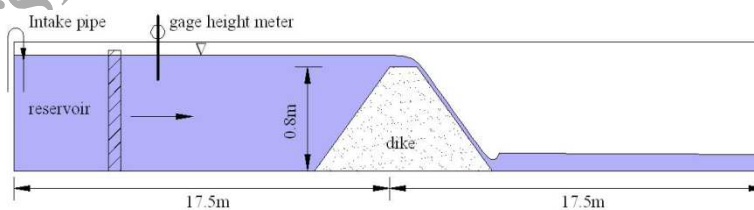


Fig.10 Schematic diagram of the experimental setup of Chinnarasri et al. (2003)

For the simulation the domain is discretised into 700 cells with $\Delta x = 0.05$ m and the bedload transport capacity is calculated by the equation of SJ or MPM according to the bed slope. As reviewed in the introduction, the Shallow Water-Exner coupled model has been frequently investigated by other researchers. To demonstrate the improvements in the model presented here, a Shallow Water-Exner coupled model proposed by Murillo and Garcia-Navarro (2010) (Murillo and Garcia-Navarro, 2010) is applied to simulate this case in order to provide comparison. Fig.11 illustrates the measured and simulated dam profiles with

three different settling velocity of particles ($\omega_0$= 0.015, 0.017 and 0.02) at t = 30 s and t = 60 s. Overall, at t = 30 s, the model predicts a bed profile fitting the measured fairly well; a reasonably good agreement is also achieved at t = 60 s, but a significant discrepancy is observed at the top of the dam. A scour hole occurs in the observation, yet this area is smooth in the numerical result and more severe scour is simulated at the downstream of dyke crest. Furthermore, the comparisons of the reservoir level and overtopping discharge are demonstrated in Fig.12. It shows that the proposed model predicts fairly good water levels, especially for $\omega_0$ = 0.017 m/s and an occurrence time of peak flow, but discrepancy from the measured data is observed for overtopping discharge. The model is found to predict a smaller peak value but larger discharge at the falling stage. As above, this is probably caused by the empirical parameters. The Shallow Water-Exner model not only underestimates the peak discharge, but simulates a quicker arrival time. The Manning's coefficient $n$ = 0.016, 0.018 and 0.02 are used to investigate its sensitivity. Fig.13 that the larger Manning's $n$ generates faster erosion, resulting a higher outflow discharge. This is due to the larger $n$ value elevating the bed shear stress, resulting in more severe scour. Although the suspension parameter $Z = \omega/(\kappa u_*)$ has been recognised and commonly used in the research community, it still cannot be estimated accurately because of a series of uncertainty factors in sediment transport. Van Rijn (1984) suggested a factor larger than 1 in that formulation as $Z = \omega/(\chi\kappa u_*)$. To investigate the sensitivity of the weighting coefficient, $\chi$ = 0.8, 1.0 and 1.2 were used to simulate the event. Fig.14 shows that the simulated beds have no significant difference because the weighting coefficient $\alpha$ is calculated as 0 on the dam crest top before peak stage by the three coefficients, i.e. suspended load is dominant. The temporal and spatial portions of suspended load in total load are demonstrated in Fig.15 to analyse how the weighting coefficient varies with time and location. It shows that the portion of suspended load is closely related to flow velocity. The velocities at the climbing and peak stage of flow are predicted to be high, this lead to suspended load to be dominant in the upstream around dam. Along with the decrease of flow, suspended load becomes weak, and instead more and more bedload occurs. This also justifies that the bedload model (SWE-Exner) might be problematic to such an event.
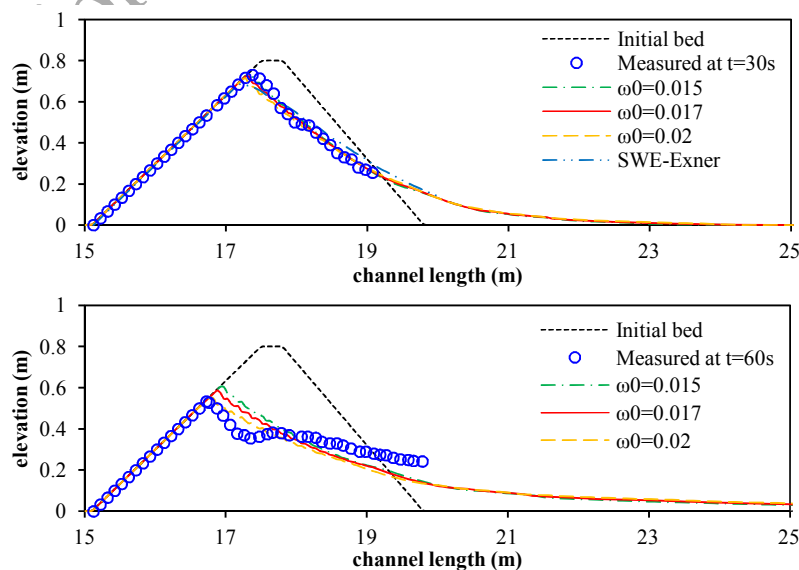


Fig.11 Simulated bed profiles for different settling velocity of sediment at t = 30 s and t = 60 s
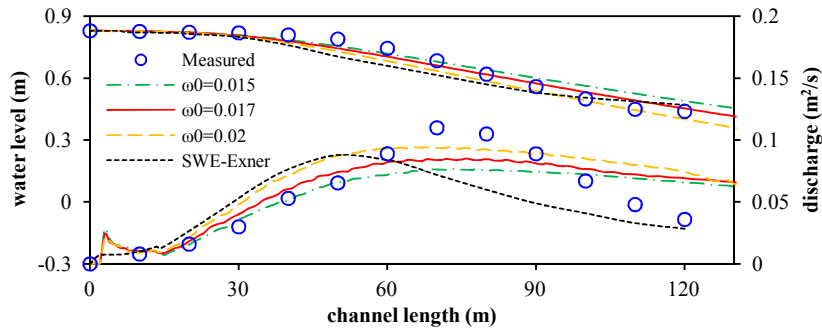
Fig.12 Simulated water level and overtopping discharge against time for the present model and SWE-Exner model
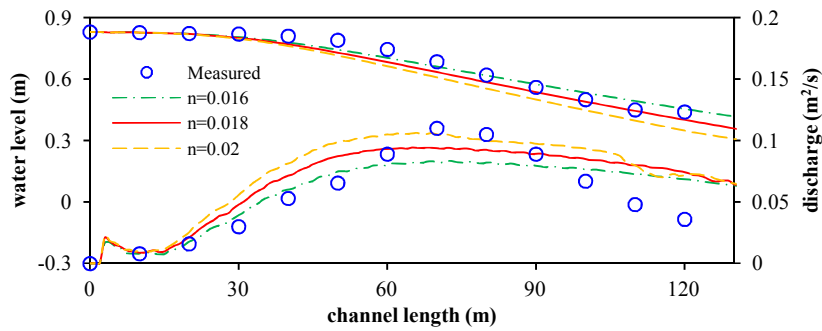


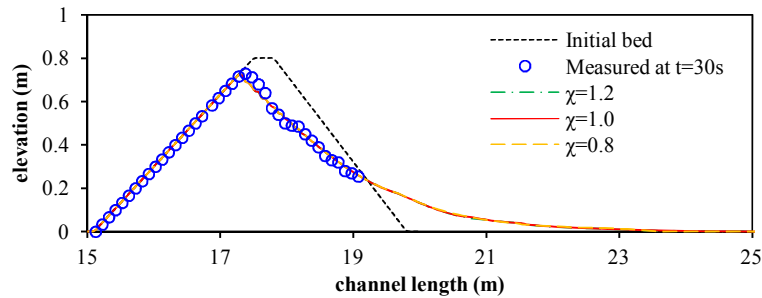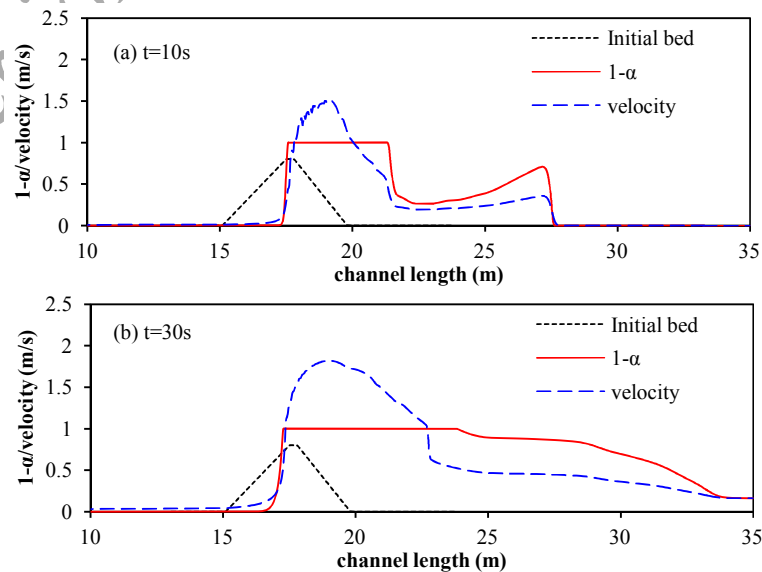Fig.13 Sensitivity of the simulated water level and overtopping discharge on Manning's $n$



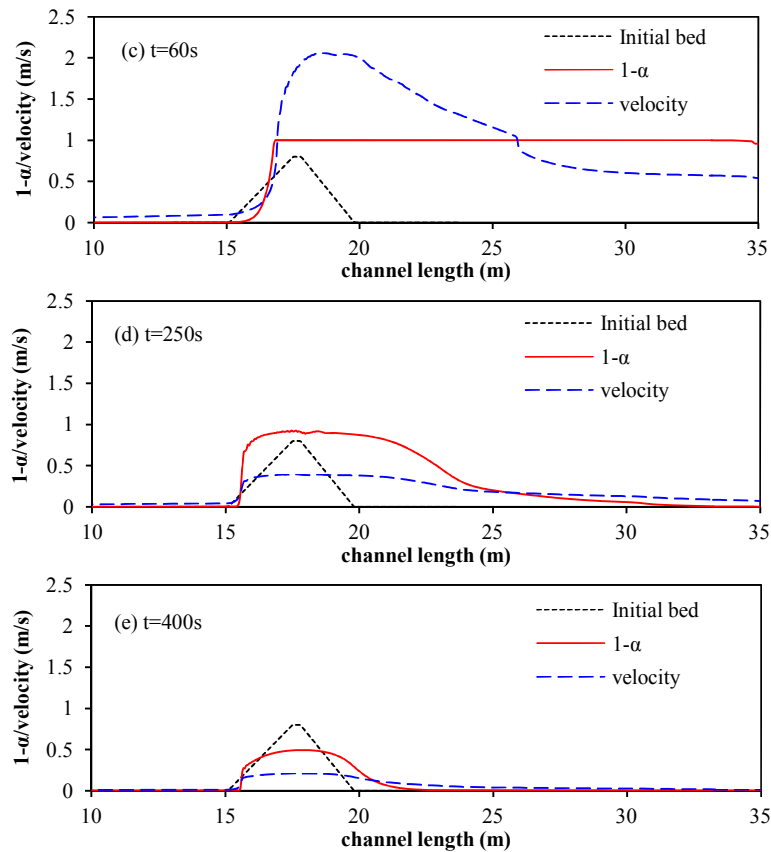Fig.14 Sensitivity test on the weighting coefficient

Fig.15 Temporal and spatial evolution of the weighting coefficient

In addition, compared to the Shallow Water-Exner model, the flexible sediment transport model can predict the spatial and temporal distribution of sediment concentration which is an important factor in understanding the erosion and deposition process. Fig.16 illustrates the sediment concentration at t = 30 s, 100 s, 150 s, 200 s and 1000 s. It is clear that the sediment concentration is larger at 30*s*, before decreasing and moving downward. As the flow becomes weak and tends towards steady state, the sediment concentration diminishes progressively in the erosion and deposition area. This test emphasizes the advantages of the multi-model morphodynamic model system in solving morphological evolution caused by complex flows. The results demonstrate that the model can predict the hydraulic and sediment information with good agreement.
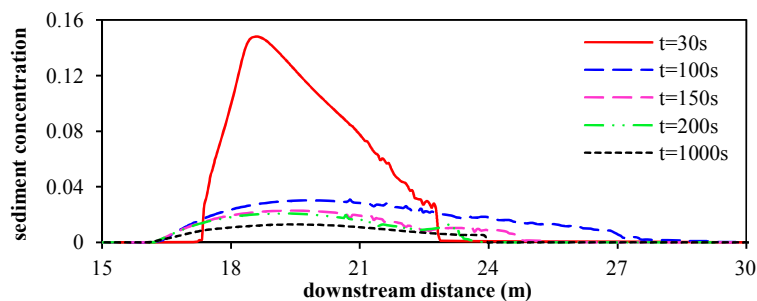


Fig.16 Depth-averaged sediment concentration at t = 30 s, 100 s, 150 s, 200 s, and 1000 s

## Conclusions

For modelling morphological change, empirical parameters are necessary. The proposed model system is no exception and inevitably, these empirical parameters may influence the results to different extents. The important parameters involve: (1) Manning's coefficient $n$. Manning's coefficient affects not only the flow values, but also the bed shear stress which induces the motion of sediment. (2) Empirical bedload capacity. This parameter was empirically produced based on the experimental data, and each formulation has its own scope of application. This parameter has significant impact on the results of any simulation. (3) The entrainment flux of suspended load. There is also no universal function available for this parameter. (4) The weighting coefficient of bedload transport. The exact value of this parameter is hitherto hard to estimate for practical engineering problems.

In conclusion, a multi-mode morphodynamic model system based on shallow water theory and non-equilibrium sediment load assumptions has been implemented. The study proposes a flexible sediment transport model which can adaptively choose an appropriate transport mode according to the local flow conditions. This makes the model not only applicable to solely bedload transport or suspended load transport, but also suitable for total mixed sediment transport with various weights of bedload and suspended load. Some key sediment parameters or relationships are identified for simulation of applicability to real hydraulic features. As shown by comparisons with experimental investigations, good agreements have been achieved, revealing that the model system presented is capable of effectively simulating flow-sediment transport events under steady or unsteady flow conditions over a flat bed or steep bed.

## References

Armanini, A., and Di Silvio, G. (1988). "A one-dimensional model for the transport of a sediment mixture in non-equilibrium conditions." *Journal of Hydraulic Research*, 26(3), 275-292, 10.1080/00221688809499212.

Bakhtyar, R., Yeganeh-Bakhtiary, A., Barry, D. A., and Ghaheri, A. (2009). "Two-phase hydrodynamic and sediment transport modeling of wave-generated sheet flow." *Advances in Water Resources*, 32(8), 1267-1283, http://dx.doi.org/10.1016/j.advwatres.2009.05.002.

Benkhaldoun, F., Sahmim, S., and Seaïd, M. (2010). "A two-dimensional finite volume morphodynamic model on unstructured triangular grids." *International Journal for Numerical Methods in Fluids*, 63(11), 1296-1327, http://dx.doi.org/10.1002/fld.2129.

Cao, Z. X., Li, Y. T., and Yue, Z. Y. (2007). "Multiple time scales of alluvial rivers carrying suspended sediment and their implications for mathematical modeling." *Advances in Water Resources*, 30(4), 715-729, http://dx.doi.org/10.1016/j.advwatres.2006.06.007.

Capart, H. (2000). "Dam-break induced geomorphic flows and the transition from solid- to fluid-like behaviour across evolving interfaces." *PhD thesis, University Catholique de Louvain, Belgium*,

Capart, H., and Young, D. L. (1998). "Formation of a jump by the dam-break wave over a granular bed." *Journal of Fluid Mechanics*, 372, 165-187, http://dx.doi.org/10.1017/S0022112098002250

Carrivick, J. L., Manville, V., Graettinger, A., and Cronin, S. J. (2010). "Coupled fluid dynamics-sediment transport modelling of a Crater Lake break-out lahar: Mt. Ruapehu, New Zealand." *Journal of Hydrology*, 388(3-4), 399-413, 10.1016/j.jhydrol.2010.05.023.

Chinnarasri, C., Tingsanchali, T., Weesakul, S., and Wongwises, S. (2003). "Flow patterns and damage of dike overtopping." *International Journal of Sediment Research*, 18(4), 301-309,

Diaz, M. J. C., Fernandez-Nieto, E. D., and Ferreiro, A. M. (2008). "Sediment transport models in Shallow Water equations and numerical approach by high order finite volume methods." *Computers & Fluids*, 37(3), 299-316, http://dx.doi.org/10.1016/j.compfluid.2007.07.017.

Dong, P., and Zhang, K. (1999). "Two-phase flow modelling of sediment motions in oscillatory sheet flow." *Coastal Engineering*, 36(2), 87-109, http://dx.doi.org/10.1016/S0378-3839(98)00052-0.

Fraccarollo, L., and Capart, H. (2002). "Riemann wave description of erosional dam-break flows." *Journal of Fluid Mechanics*, 461, 183-228, http://dx.doi.org/10.1017/S0022112002008455.

Greimann, B., Lai, Y., and Huang, J. C. (2008). "Two-dimensional total sediment load model equations." *Journal of Hydraulic Engineering-ASCE*, 134(8), 1142-1146, http://dx.doi.org/10.1061/(ASCE)0733-9429(2008)134:8(1142).

Guan, M. F., Wright, N. G., and Sleigh, P. A. (2013) "Modelling and understanding multiple roles of sediment transport in floods." *Proc., 35th IAHR World Congress*, Tsinghua University Press.

Guan, M. F., Wright, N. G., and Sleigh, P. A. (2013). "A robust 2D shallow water model for solving flow over complex topography using homogenous flux method." *International Journal for Numerical Methods in Fluids*, 73(3), 225-249, 10.1002/fld.3795.

Guan, M. F., Wright, N. G., and Sleigh, P. A. (2014). "2D Process based Morphodynamic Model for Flooding by Non-cohesive Dyke Breach." *Journal of Hydraulic Engineering-ASCE,* http://dx.doi.org/10.1061/(ASCE)HY.1943-7900.0000861.

Jenkins, J. T., and Hanes, D. M. (1998). "Collisional sheet flows of sediment driven by a turbulent fluid." *Journal of Fluid Mechanics*, 370, 29-52, http://dx.doi.org/10.1017/S0022112098001840

Lamb, M. P., Dietrich, W. E., and Venditti, J. G. (2008). "Is the critical Shields stress for incipient sediment motion dependent on channel-bed slope?" *Journal of Geophysical Research-Earth Surface*, 113(F2), F02008 10.1029/2007jf000831.

Lee, S.-H., and Wright, N. G. (2010). "Simple and efficient solution of the shallow water equations with source terms." *International Journal for Numerical Methods in Fluids*, 63(3), 313-340, 10.1002/fld.2071.

Li, M., Pan, S., and O'Connor, B. A. (2008). "A two-phase numerical model for sediment transport prediction under oscillatory sheet flows." *Coastal Engineering*, 55(12), 1159-1173, http://dx.doi.org/10.1016/j.coastaleng.2008.05.003.

Li, S. C., and Duffy, C. J. (2011). "Fully coupled approach to modeling shallow water flow, sediment transport, and bed evolution in rivers." *Water Resources Research*, 47, W0350810.1029/2010wr009751.

Meyer-Peter, E., and Müller, R. (1948). "Formulas for bed load transport." *Proc., 2nd Meeting*Stockholm, Sweden, 39–64.

Murillo, J., and Garcia-Navarro, P. (2010). "An Exner-based coupled model for two-dimensional transient flow over erodible bed." *Journal of Computational Physics*, 229(23), 8704-8732, http://dx.doi.org/10.1016/j.jcp.2010.08.006.

Parker, C., Clifford, N. J., and Thorne, C. R. (2011). "Understanding the influence of slope on the threshold of coarse grain motion: Revisiting critical stream power." *Geomorphology*, 126(1-2), 51-65,

http://dx.doi.org/10.1016/j.geomorph.2010.10.027.

Phillips, B. C., and Sutherland, A. J. (1989). "Spatial lag effects in bed-load sediment transport." *Journal of Hydraulic Research*, 27(1), 115-133, 10.1080/00221688909499247.

Pugh, F. J., and Wilson, K. C. (1999). "Velocity and concentration distributions in sheet flow above plane beds." *Journal of Hydraulic Engineering-ASCE*, 125(2), 117-125, 10.1061/(asce)0733-9429(1999)125:2(117).

Seal, R., Paola, C., Parker, G., Southard, J. B., and Wilcock, P. R. (1997). "Experiments on downstream fining of gravel .1. Narrow-channel runs." *Journal of Hydraulic Engineering-ASCE*, 123(10), 874-884, http://dx.doi.org/10.1061/(ASCE)0733-9429(1997)123:10(874).

Simpson, G., and Castelltort, S. (2006). "Coupled model of surface water flow, sediment transport and morphological evolution." *Computers & Geosciences*, 32(10), 1600-1614, 10.1016/j.cageo.2006.02.020.

Singh, V. P. (1996). *Dam Breach Modeling Technology*, Kluwer Academic, the Netherlands.

Smart, G., and Jäggi, M. (1983). "Sediment transport on steep slopes." *Mitteilung. 64. Versuchsanstalt fü r Wasserbau, Hydrologie und Glaziologie, ETH Zurich, Zurich*,

Soulsby, R. (1997). *Dynamics of marine sands: a manual for practical applications*, ThomasTelford, London, UK.

Spasojevic, M., and Holly, M. (2008). "Two- and Three-Dimensional Numerical Simulation of Mobile-Bed Hydrodynamics and Sedimentation." *Sedimentation engineering: processes, measurements, modeling, and practice*, H. G. Marcelo, ed., American Society of Civil Engineers, 683-761.

Spinewine, B. (2005). "Two-layer flow behaviour and the effects of granular dilatancy in dam-break induced sheet-flow." *PhD thes*is, Univerisité catholique de Louvain, Belgium.

Spinewine, B., and Zech, Y. (2007). "Small-scale laboratory dam-break waves on movable beds." *Journal of Hydraulic Research*, 45, 73-86, 10.1080/00221686.2007.9521834.

Sumer, B. M., Kozakiewicz, A., Fredsoe, J., and Deigaard, R. (1996). "Velocity and concentration profiles in sheet-flow layer of movable bed." *Journal of Hydraulic Engineering-ASCE*, 122(10), 549-558, http://dx.doi.org/10.1061/(ASCE)0733-9429(1996)122:10(549).

van Rijn, L. C. (1984). "Sediment transport part I, bed load transport." *Journal of Hydraulic Engineering-ASCE*, 110(10), 1431-1456, http://dx.doi.org/10.1061/(ASCE)0733-9429(1984)110:10(1431).

van Rijn, L. C. (1984). "Sediment transport part II, suspended load transport." *Journal of Hydraulic Engineering-ASCE*, 110 (11), 1613–1641, http://dx.doi.org/10.1061/(ASCE)0733-9429(1984)110:11(1613).

Wu, W., Marsooli, R., and He, Z. (2012). "Depth-Averaged Two-Dimensional Model of Unsteady Flow and Sediment Transport due to Noncohesive Embankment Break/Breaching." *Journal of Hydraulic Engineering*, 138(6), 503-516, doi:10.1061/(ASCE)HY.1943-7900.0000546.

Wu, W. M. (2004). "Depth-averaged two-dimensional numerical modeling of unsteady flow and nonuniform sediment transport in open channels." *Journal of Hydraulic Engineering-ASCE*, 130(10), 1013-1024, http://dx.doi.org/10.1061/(ASCE)0733-9429(2004)130:10(1013).

Wu, W. M., and Wang, S. S. Y. (2008). "One-dimensional explicit finite-volume model for sediment transport with transient flows over movable beds." *Journal of Hydraulic Research*, 46(1), 87-98,

Zech, Y., Soares-Frazao, S., Spinewine, B., and Grelle, N. L. (2008). "Dam-break induced sediment movement: Experimental approaches and numerical modelling." *Journal of Hydraulic Research*, 46(2), 176-190, 10.1080/00221686.2008.9521854.